Integrated Assembly and Photopreservation of Topographical Micropatterns

Shuailong Zhang[1,2,3], Weizhen Li[4], Mohamed Elsayed[1,3], Jiaxi Peng,[1,2,3] Yujie Chen[5], Yanfeng Zhang[5], Yibo Zhang[6], Moein Shayegannia,[6] Wenkun Dou,[7] Tiancong Wang,[7] Yu Sun,[3,6,7] Nazir P. Kherani[6,8], Steven L. Neale[4] and Aaron R. Wheeler[1,2,3,*]

1. *Donnelly Centre for Cellular and Biomolecular Research, University of Toronto, Toronto, ON, Canada M5S 3E1*
2. *Department of Chemistry, University of Toronto, Toronto, ON, Canada M5S 3H6*
3. *Institute of Biomedical Engineering, University of Toronto, Toronto, ON, Canada M5S 3G9*
4. *James Watt School of Engineering, University of Glasgow, Glasgow G12 8LT, UK*
5. *State Key Laboratory of Optoelectronic Materials and Technologies, School of Electronics and Information Technology, Sun Yat-sen University, Guangzhou 510275, China*
6. *Department of Electrical and Computer Engineering, University of Toronto, Toronto, ON, Canada M5S 3G4*
7. *Department of Mechanical and Industrial Engineering, University of Toronto, Toronto, M5S 3G8, Canada*
8. *Department of Materials Science and Engineering, University of Toronto, Toronto, ON, Canada M5S 3E4*

Author email addresses:

Shuailong Zhang: shuailong.zhang@utoronto.ca; Weizhen Li: w.li.4@research.gla.ac.uk; Mohamed Elsayed: mohammed.elsayed@mail.utoronto.ca; Jiaxi Peng: jiaxi.peng@mail.utoronto.ca; Yujie Chen: chenyj69@mail.sysu.edu.cn; Yanfeng Zhang: zhangyf33@mail.sysu.edu.cn; Yibo Zhang: yibojhhk.zhang@mail.utoronto.ca; Moein Shayegannia: moein.shayegannia@mail.utoronto.ca; Wenkun Dou: wenkun.dou@mail.utoronto.ca; Tiancong Wang: tiancong.wang@mail.utoronto.ca; Yu Sun: sun@mie.utoronto.ca; Nazir P. Kherani: kherani@ecf.utoronto.ca; Steven L. Neale: Steven.Neale@gla.ac.uk; Aaron R. Wheeler: aaron.wheeler@utoronto.ca;

[*]Contact details for the corresponding author:

Aaron R. Wheeler

Email: aaron.wheeler@utoronto.ca; Tel: 416-946-3866; Fax: 416-946-3865

Address: 80 St. George Street, Department of Chemistry, University of Toronto, Toronto, ON, Canada M5S 3H6

Abstract: Micromanipulation techniques that are capable of assembling nano-/micro- materials into usable structures such as topographical micropatterns (TMPs) have proliferated rapidly in recent years, holding great promise in building artificial electronic and photonic microstructures. Here we report a method for forming TMPs based on optoelectronic tweezers (OET) in either "bottom up" or "top down" modes, combined with *in situ* photopolymerisation to form permanent structures. We demonstrate that the assembled/cured TMPs can be harvested and transferred to alternate substrates, and we illustrate how permanent conductive traces and capacitive circuits can be formed, paving the way towards applications

in microelectronics. The integrated, optical assembly/preservation method described here is accessible, versatile, and applicable for a wide range of materials and structures, suggesting utility for myriad microassembly and microfabrication applications in the future.

Keywords: Optical micromanipulation, photocurable hydrogel, dielectrophoresis, carbon nanoparticles, silver nanoparticles, graphene nanoplatelets, solder microbeads, capacitive circuits, micro-electronics.

Introduction

Micro-assembly technologies have proliferated in recent years, driven by great interest in the capacity to manufacture functional micro- and nano- devices for a wide range of applications. Most of these micro-assembly technologies rely on “pick-and-place” techniques,[1-8] in which a robotic arm with a “catch-and-release” tip is used to mechanically select targeted objects to assemble them into desired combinations and geometries, which we call 'topographical micropatterns' (TMPs). These assembly techniques are useful, but they also rely on expensive and specialized positioning tools and well-trained personnel, and can be limited by material properties and throughput.

Optical assembly is an alternative strategy to assemble functional structures from micro- and nano-objects as building blocks.[9] Optical assembly relies on optical micromanipulation technologies such as optical tweezers,[9-13] opto-thermophoretic tweezers,[14-16] photovoltaic tweezers,[17-20] and optoelectronic tweezers,[21-30] in which micro- and nano- objects are optically assembled into a pattern in a fluidic environment and later dried for use in various applications. This approach has advanced rapidly in recent years, and preserves many of the advantages of the conventional methods while being easy-to-implement and allowing for cost-effective operation. Among different optical micromanipulation techniques, optoelectronic tweezers (OET) has proven to be particularly useful for the assembly of large numbers of micro- and nano- objects in parallel,[22-31] and also for the assembly of micro-objects with 'large' sizes (with at least one dimension greater than 150 microns).[32-34] However, one limitation for OET assembly (and also for other optical assembly techniques) is that the process must be performed in a fluidic environment, such that the fluid must be removed afterwards, often by evaporation, a chaotic process that can destroy the structure that has (up to that point) been carefully assembled. This problem is partly solved via a previously reported freeze-drying process, in which the liquid medium is frozen and then sublimated.[29,35] However, the freeze-drying process requires that the assembled structure be compatible with low temperatures and low pressures, which sets limitations on the materials that can be used. In addition, freeze-drying increases the time of operation and the system complexity.

Here, we report a new method of TMP assembly, using OET to assemble micro- and nano-objects into functional structures that are then preserved via *in situ* photopolymerization. This technique is enabled by a digital micromirror device (DMD) integrated with independently controlled light sources with different wavelengths, which can be used to both assemble the nano-/micro- objects and to preserve their structures via selective photopolymerization of a hydrogel solution. In this introductory report, we

demonstrate that carbon/silver nanoparticles, graphene nanoplatelets and polystyrene microbeads can be assembled into TMPs in either a "bottom up" mode, in which up to hundreds of thousands of particles are brought together in parallel (analogous to structural self-assembly) or a "top down" mode, in which particles are manipulated one-by-one (analogous to pick-and-place assembly). After formation, the TMPs are immobilized/preserved via photopolymerization and can be transferred onto a variety of flexible and rigid substrates. Most uniquely, we demonstrate how metallic microspheres can be assembled to form permanent conductive electrical traces and to assemble capacitors into working microcircuits. We propose that the new method presented here is versatile and powerful, and could be useful for a wide range of micro-assembly and micro-fabrication applications in the future.

Results and Discussion

The methods introduced here rely on OET, a technique that utilizes light-induced dielectrophresis (DEP) to manipulate nano-/micro-objects.[21,36] Similar to our previous reports,[34,37] the OET devices used here consist of two plates formed from indium tin oxide (ITO)-coated glass slides. The bottom plate was coated with an additional layer of photoconductive material – hydrogenated amorphous silicon (a-Si:H). The devices were assembled by adhering the top and bottom plates together with a spacer to form a chamber, within which the manipulation was performed by projecting patterns of light onto the a-Si:H layer to form locally conductive 'virtual electrodes' to drive DEP. In a departure from previous OET work, the system was configured to allow the DMD to control different wavelengths (including red light from a 620 nm diode and UV light from a 380 nm diode), as shown in Figure 1(a). The different wavelengths of light are focused through the objective of an upright microscope to form light patterns on the photoconductive substrate in the OET device. In this technique, the chamber of the OET device contains both the nano-/micro-objects to be manipulated as well as a sol-form of a photopolymerizable poly(ethylene glycol) diacrylate (PEGDA) hydrogel solution. When red light is projected into the OET device and an AC bias is applied, the device operates in OET mode, in which nano-/micro-objects are manipulated and assembled, and when UV light is projected into the device, the system operates in ‘gel-curing’ mode, in which the hydrogel solution is polymerized. After the polymerization, a solid structure is formed and the assembled nano-/micro-structures are immobilized and encapsulated in the solid structure.

We are aware of three previous reports describing the use of OET[38], optical tweezers[39] or opto-thermophoretic tweezers[40] to assemble particles into microstructures that were subsequently immobilized by photopolymerization. Two of these methods[39-40] were limited to "top down" assembly of structures from fewer than ten particles, and in all of them, the photopolymer did not have a particular structure – it was just a shapeless 'carrier' used to immobilize the assembled particles. Here, we introduce a new strategy in which the photopolymer is also formed into defined shapes, making use of the same DMD which is used to control the OET/DEP forces (see below), to enhance the ultimate utility of the finished products. Supplementary Movie S1 (clip 1) and Figure 1(b)-(d) illustrate the process of forming a photopolymerized structure – in this case, a 3D outline of a ‘maple leaf’. As shown, when the

appropriate pattern is projected into the device, the pre-polymer solution becomes cross-linked (only in regions exposed to UV light), and the solid structures become cured in around 5 seconds, after which the remaining pre-polymer solution can be rinsed away. Using the DMD allows for straightforward generation of photopolymerized structures with controllable geometries, selected on demand. For example, supplementary movie S1 (clips 2-6) and Figure 1(e)-(j) show examples of different geometries (cartoons, numbers, letters, symbols and shapes) that can be formed. As described in the supplementary information file (and as illustrated in Figure S1), the process is straightforward with a user-friendly computer interface, making this technique easy to teach to new users. After forming the microstructures, they can subsequently be extracted and used for a variety of applications; for example, scanning electron microscope (SEM) images of three of the structures are shown in Figure 1(k)-(m). Although the DMD projection-photopolymerization method described here has poorer resolution than that of other maskless lithography techniques such as two-photon polymerization[41] and dip-pen lithography,[42] it offers a number of advantages, including relatively high throughput, user-friendly operation, and compatibility with enclosed systems. Note that the height of polymerized structures in the current system is defined by the chamber dimensions; in the future, more precise Z-axis control might be possible by integration with two-photon techniques.[41]

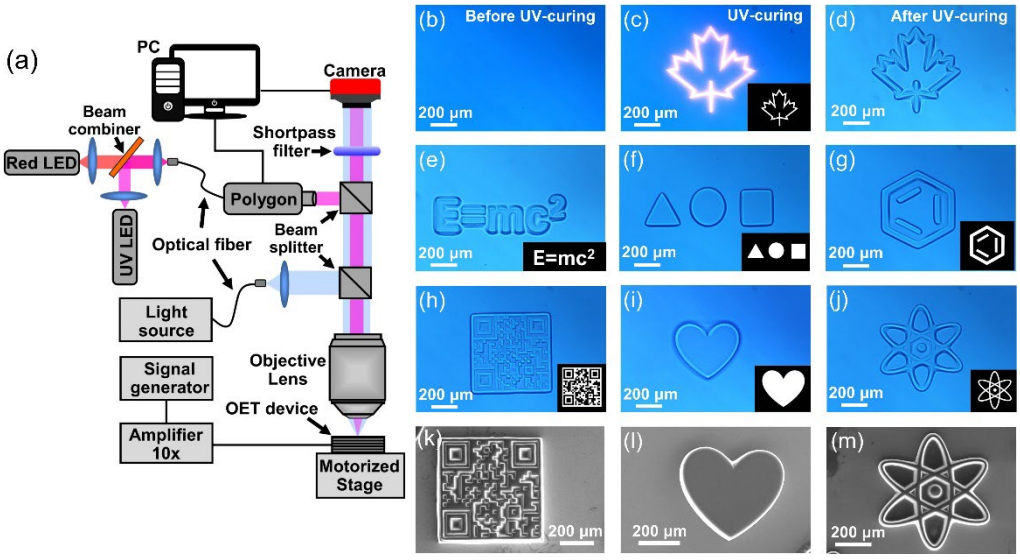

Figure 1. Experimental setup and polymerized hydrogel structures. (a) Schematic of the experimental setup, featuring LEDs with two wavelengths (red: 620 nm; UV: 380 nm) that can be controlled by a Polygon DMD (Mightex Inc.). (b)-(d) Bright-field microscope images (frames from Movie S1) demonstrating the UV photopolymerization process of sol-form hydrogel solution (concentrated PEGDA) to form a 3D microstructure of an outline of a 'maple leaf'. Bright-field microscope images (many from frames of Movie S1) of cured hydrogel microstructures in the form of (e) the mass-energy equation, (f) a triangle, circle, and square, (g) the chemical symbol for benzene, (h) a quick response (QR) code, (i) a 'heart' symbol, and (j) an 'atom' symbol. The insets are the black and white images that were projected into the device to generate the cured hydrogel microstructures. Representative SEM images of cured hydrogel microstructures, showing the (k) QR code, (l) 'heart' symbol, and (m) 'atom' symbol.

The concentrated PEGDA solution used to form the structures in Figure 1 has high viscosity, which hampers manipulation of particles suspended in that solution by OET. To identify conditions that allow both UV-curing and OET manipulation, dilutions of concentrated PEGDA solution in DI water were formed (1:1, 1:2, 1:3, 1:4, and 1:5), and each was tested and evaluated based on the performance of OET manipulation and UV curing. Supplementary movie S2 and Figure 2(a-b) illustrate a typical OET manipulation experiment: a doughnut-shaped light pattern (red) is projected into a sol-form PEGDA solution to move a 10 μm diameter polystyrene microbead. In these experiments, the OET device was driven at an AC bias of 15 Vpp at 20 kHz, which generated a negative DEP force that caused the particle to remain within the dark region of the doughnut (in cases in which the DEP force was greater than viscous drag). The maximum moving velocities as well as the percentage of movable polystyrene microbeads were measured in different dilutions of concentrated PEGDA to DI water. As shown in Figure 2(c), both properties increase as PEGDA concentration decreases, likely because of reduced viscosity.

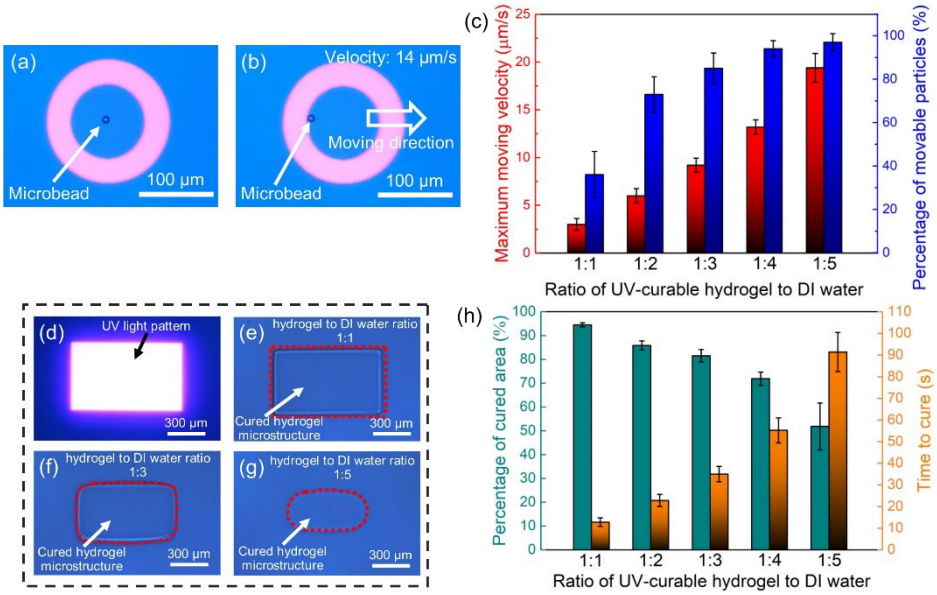

Figure 2. OET particle movement and UV-curable hydrogel curing. Bright-field microscope images (frames from Movie S2) of (a) trapping a 10 μm dia. polystyrene microbead and (b) moving the bead at 14 μm/s using a doughnut-shaped light pattern. The white arrow indicates the direction of movement. (c) Plots of maximum moving velocity (left, red) and the percentage of movable polystyrene particles (right, blue) in solutions with different dilutions of concentrated PEGDA solution in DI water. Error bars represent standard deviation for five replicates. Bright-field microscope images illustrating the results of projecting a rectangular-shaped UV light pattern (d) to cure solutions with 1:1 (e), 1:3 (f), and 1:5 (g) dilutions of concentrated PEGDA solution in DI water. The boundaries of the cured materials in (e-g) are highlighted with red dotted outlines. (h) Plots of the percentage of cured hydrogel (left, teal, from areas measured relative to the projected UV light pattern) and the required curing time (right, orange) in solutions with different dilutions of concentrated PEGDA solution in DI water. Error bars represent standard deviation for five replicates.

Each PEGDA dilution was also evaluated for curing properties when exposed to UV light. For example, Figures 2(d)-(g) are bright-field microscopy images of the illumination of different PEGDA solutions with a rectangular- UV light pattern. As shown in Figure 2(h), the percentage of the cured area (compared to the area of the UV light pattern) decreases with a decreasing ratio of concentrated PEGDA, and the time required for the solution to cure increases with a decreasing ratio of concentrated PEGDA. Therefore, a trade-off exists between OET particle manipulation performance and UV curing performance when choosing the dilution of concentrated PEGDA. Based on the results in Figure 2(c) and 2(h), a ratio of 1:4 concentrated PEGDA solution to DI water was selected to ensure both effective particle manipulation and UV photopolymerization. This ratio was used for all of the experiments described below.

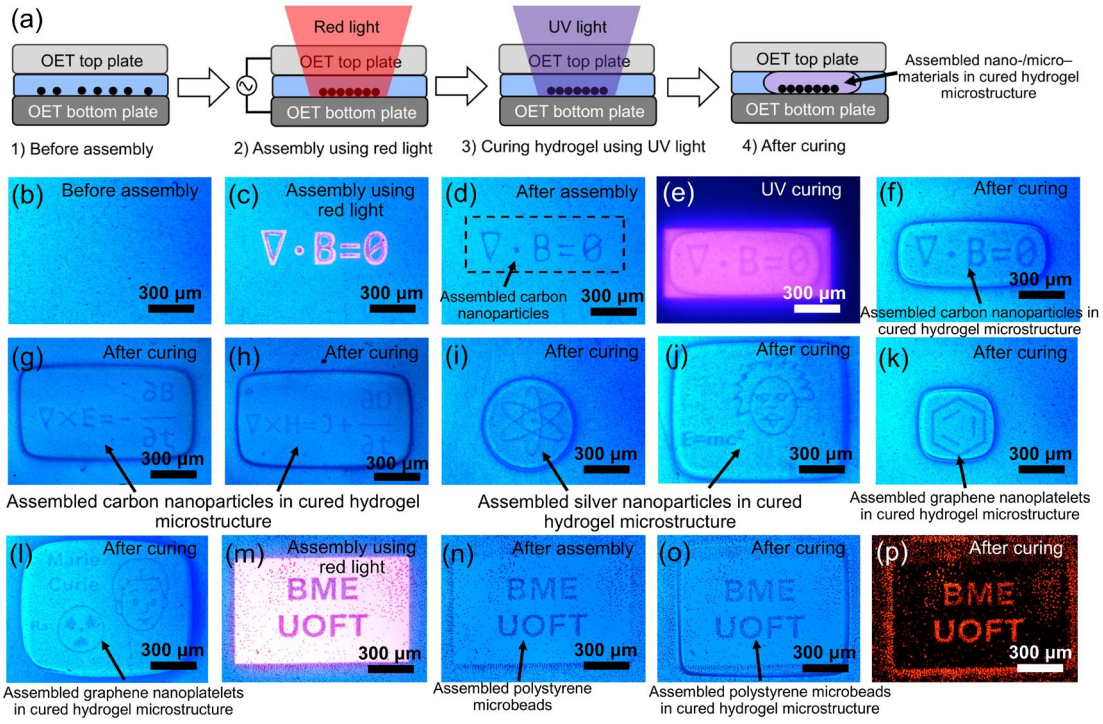

Figure 3. Assembly of nano-/micro-materials into TMPs in bottom-up mode and preservation of the assembled TMPs via UV photopolymerization in concentrated PEGDA diluted 1:4 in DI water. (a) Schematic process of OET assem6bly via red light and solution curing via UV light. Bright-field microscopy images of carbon nanoparticles (b) before OET assembly, (c) during OET assembly (d) after OET assembly, (e) during UV curing, and (f) after UV curing of a TMP featuring the differential form of Gauss's Law for Magnetism. Bright-field microscopy images of assembled/cured carbon nanoparticle TMPs featuring (g) the differential form of Faraday's Law and (h) the differential form of the Ampere-Maxwell Law, assembled/cured silver nanoparticle TMPs depicting (i) the 'atom' symbol and (j) a stylized caricature of Albert Einstein with the mass energy equation, and assembled/cured graphene nanoplatelet TMPs depicting (k) the chemical symbol for benzene and (l) a stylized caricature of Marie Curie with the symbol for radioactivity. Bright-field microscopy images of 6 μm diameter fluorescent polystyrene microbeads (m) during OET assembly, (n) after OET assembly, and (o) after UV curing of a TMP featuring the text "BME UOFT" (abbreviation for biomedical engineering at the University of Toronto). (p) Fluorescence microscopy image of the assembled/cured TMP formed in (m-o).

After determining an optimum ratio of concentrated PEGDA to DI water in the solution, experiments were carried out to explore the capacity to assemble up to hundreds of thousands of nano-/micro-particles into TMPs in bottom-up mode followed by preserving them in cured hydrogel structures. Figure 3(a) illustrates the step-by-step procedure of using red and UV light patterns to assemble nano-/micro-materials into TMPs and preserve the assembled TMPs via photopolymerization. (Note that this example illustrates particles that are conductive and experience positive DEP force, drawing the particles into the illuminated region.) Figure 3(b)-(f) shows representative microscope images of each step of this process for a suspension of carbon nanoparticles (which experience positive DEP) [Figure 3(b)] being assembled into a TMP depicting the differential form of one of the Maxwell equations, Gauss's Law for Magnetism [Figure 3(c)-(d)], and then being preserved in a cured hydrogel [Fig. 3(e)-(f)]. Note that the TMP remains unchanged during the photopolymerization, suggesting that potentially disruptive forces caused by UV curing have little influence on the assembled TMP. In general, as illustrated in supplementary Movie S3, TMPs formed in this "bottom up" manner feature millions (or more) particles that are simultaneously assembled, in a process that requires ~40 seconds of red light projection and ~50 seconds of UV light projection. We have used carbon nanoparticles [Figure 3(g)-(h)], silver nanoparticles [Figure 3(i)-(j)], and graphene nanoplatelets [Figure 3(k)-(l)] (all of which experience positive DEP) to form TMPs representing an assortment of Maxwell's equations, cartoons and chemical formulas, and stylized caricatures of famous scientists. TMPs can also be formed from dielectric particles that experience negative DEP (via negative red-light patterns), such as polystyrene beads [Fig. 3(m)-(o)], which (in this example) happen to be fluorescent [Figure 3(p)]. The design-possibilities are nearly endless, with additional examples of TMPs found in Figure S2, and can be formed from diverse micro/nano materials with a wide range of sizes and shapes, as shown in the SEM images in Figure S3.

After demonstrating the capability for (i) assembling TMPs with different designs and different materials using OET, and (ii) immobilizing/preserving the assembled TMPs via UV photopolymerization, we investigated the feasibility of transferring the assembled/cured TMPs in hydrogel microstructures to other substrates. We used a technique described previously for moving freeze-dried structures,[29] in which two destination-substrates were used for transfer: polydimethylsiloxane (PDMS) and double-sided adhesive tape. A schematic illustrating the process of transferring assembled/cured TMPs in hydrogel microstructures to the two kinds of substrates is shown in Figure 4(a). Images illustrating various stages of transfer for both kinds of substrate are shown in Figure 4(b-h). During the transfer process, the PDMS substrate functions as an elastomeric stamp which attracts the cured hydrogel microstructures (bearing encapsulated TMPs) by kinetic adhesion;[2] likewise, the chemical adhesive on the double-sided tape allows for capture of cured hydrogel microstructures (with encapsulated TMPs). The transferred hydrogel microstructures and the encapsulated TMPs are robust, such that they can withstand touching and bending. These results demonstrate proof-of-concept for the harvest and transfer of TMPs to other acceptor substrates/surfaces, with the potential to serve as anti-counterfeiting markers for official documentation,[29] novelty micrologos for exhibitions or conferences, or (in combination with educational materials related to the principles of DEP and OET and Movie S3) as activities and support

for classroom/laboratory instruction.[43] Importantly, none of the previous reports describing photocured TMPs[38-40] described the capacity to transfer the structures after photopolymerization or to use them in any way. This was a key goal in the work described here.

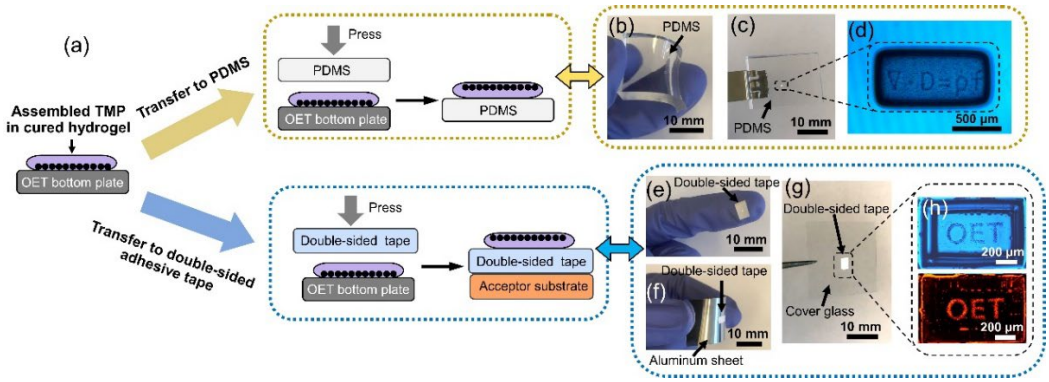

Figure 4. Transfer of assembled/cured TMPs to destination substrates. (a) Schematic illustration of transferring TMPs encapsulated in cured hydrogel microstructures (formed in concentrated PEGDA diluted 1:4 in DI water) to PDMS (gray, in yellow-dashed box), and double-sided adhesive tape (blue, in blue-dashed box) substrates. The latter (double-sided tape) is then mounted on an acceptor substrate (orange). (b)-(c) Images of PDMS substrates bearing assembled, cured, and transferred TMPs. (d) Microscope image of a TMP depicting the differential form of Gauss's law for electric fields in a cured hydrogel microstructure after transfer to a PDMS substrate. Images of double-sided tape substrates bearing assembled/cured TMPs mounted on (e) a glove, (f) a flexible aluminum sheet, and (g) a cover glass. (h) Bright-field (top) and fluorescence (bottom) microscopy images of cured/assembled TMP featuring the text "OET" (abbreviation for optoelectronic tweezers) after transfer to a double-side tape substrate.

As a test-case for using TMPs formed by the techniques described here, we decided to evaluate the potential for forming working microelectronic circuits. As a first step towards this goal, we evaluated the capacity to manipulate conductive $Sn_{62}Pb_{36}Ag_2$ solder beads, which have spherical structures with sizes ranging from 15 μm to 25 μm. Like carbon nanoparticles, silver nanoparticles, and graphene nanoplatelets, the solder beads used here experience a positive DEP force. Based on Stokes' Law, the viscous drag force F_{Drag} of a trapped particle can be calculated, which can be used to estimate the DEP force F_{DEP} that the particle experiences:

$$F_{DEP} = F_{Drag} = 6\pi\eta r v \quad (1)$$

where η is the viscosity of the solution, r is the radius of the solder bead and v is velocity of the particle. Supplementary Movie S4 and Figure 5(a)-(b) illustrate the translation of a 20 μm diameter solder bead using a circular light pattern at 20 μm/s and 60 μm/s. As shown, the center-to-center distance [D in Figure 5(a)-(b)] between the bead and the light pattern increases with an increasing velocity and F_{Drag}. By measuring the center-to-center distance at varying velocities, a profile of the DEP force experienced by a bead at different positions within the trap can be plotted, as shown by the markers in Figure 5(c). We also investigated the achievable positioning accuracy of solder beads[47], which is important for

assembly applications. Solder beads were repeatedly translated to randomized destinations between 30-500 µm away from their initial positions, and the difference between each bead's relative position in the trap before and after moving, the "post-translational offset" (PTO), was recorded. The PTOs observed for 18 different beads are shown in Figure 5(d), with average absolute X- and Y-values found to be 0.71 µm and 0.69 µm, respectively. Thus, this method, which relies on a 30-µm-diameter OET trap, allows for sub-micron positioning accuracy for manipulating solder beads.

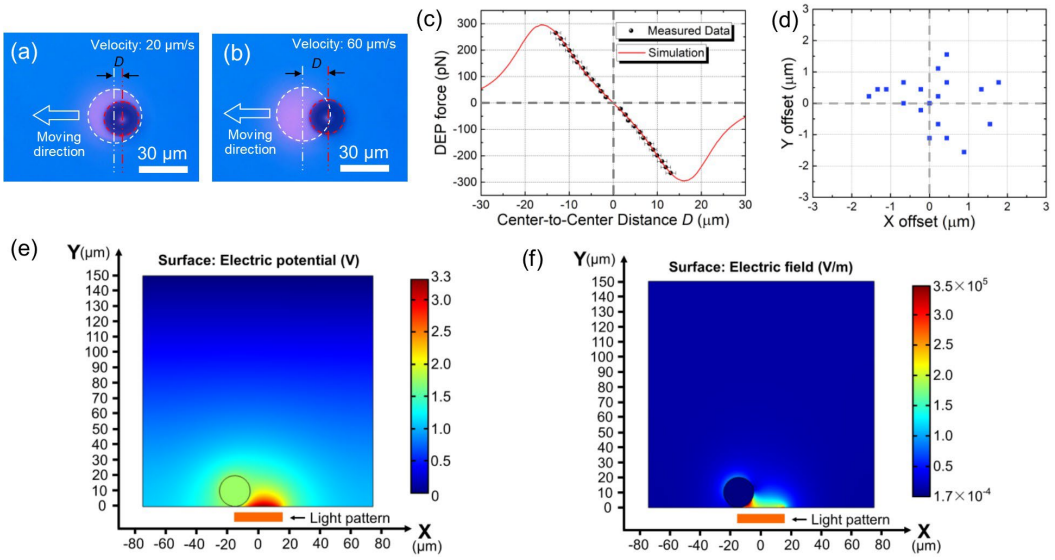

Figure 5. OET manipulation of solder beads. Bright-field microscope images (frames from movie S4) illustrating the translation of a 20 µm diameter solder bead at (a) 20 µm/s, and (b) 60 µm/s using a 30-µm-diamater circular light pattern (from supplementary Movie S4) in concentrated PEGDA diluted 1:4 in DI water. The white arrow indicates the direction of movement. (c) Measured trap profile (markers) and simulated trap profile (by Maxwell stress tensor, solid red line) for the conditions illustrated by (a)-(b). Error bars represent standard deviation for 10 replicates per condition. (d) Post-translation offsets measured for 18 solder beads in concentrated PEGDA diluted 1:4 in DI water before and after movement at least 30 µm. Simulated distribution of (e) electric potential, and (f) electric field in an OET device with a solder bead positioned at the left edge of the trap, formed by illuminating a 30-µm-diameter circular light pattern (shaded in orange) onto the a-Si:H surface (at Y = 0). The simulated electric potential and field are indicated in heat maps (blue = low, red = high) and the solder bead is illustrated as a hollow black circle.

To further analyze the performance of OET manipulation of the solder bead, the trap profile was simulated in COMSOL Multiphysics based on a 3D model (Fig. S4). Simulated profiles of electric potential and field are shown in Figure 5(e)-(f). As indicated, these properties (an in particular the field) vary substantially across the solder bead, which makes the assumption (that is often made in DEP simulations) that the field is invariant with respect to the trapped particle inappropriate. Thus, a numerical estimate of DEP force on the particle F_{DEP} was generated by integrating the Maxwell stress tensor over the surface of the bead, a method described previously[48,49] for approximating behavior in systems in

which a trapped particle causes substantial perturbation to the applied electric field. Details of the simulation are in the supplementary information file, and as shown by the red plot in Figure 5(c), the result has good qualitative agreement with experimental observations.

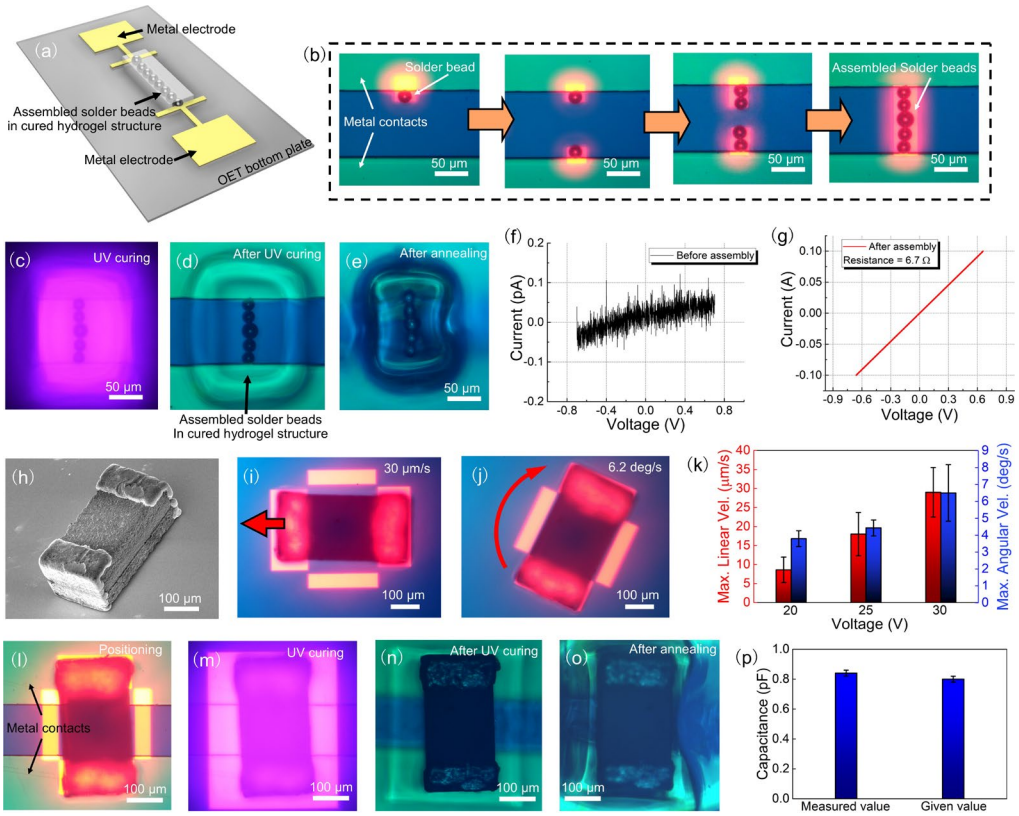

Figure 6. Top-down assembly of microelectronic circuits and preservation via UV photopolymerization. (a) Schematic of OET-assembled solder beads (grey) in cured hydrogel connecting two metal electrodes (yellow) on an OET bottom plate. (b) Bright-field microscopy images (frames from Movie S5, left-to-right), illustrating the process of using OET to manipulate five solder beads into position to bridge a gap between electrodes. Images of the assembled solder beads from (b) while curing (c), after curing (d), and after annealing (e). I-V measurements of metal contacts (f) before and (g) after being connected by an OET-assembled conductive trace (and then cured and annealed). (h) SEM image of a microcapacitor. Bright-field microscope images (frames from Movie S6), illustrating the process of using OET to (i) move the capacitor at 30 μm/s, and (j) rotate the capacitor at 6.2 rad/s, with red arrows indicating the direction of motion. (k) Plot of maximum linear velocity (left axis, red) and angular velocity (right axis, blue) of microcapacitors as a function of bias voltage. Error bars represent standard deviation for 5 replicates. Bright-field microscopy images of illustrating a microcapacitor after positioning between two electrodes (l), while curing (m), after curing (n), and after annealing (o). Capacitance measurements of electrodes (f) before and (g) after being connected by an OET-positioned capacitor (and then cured and annealed). Error bars for measured value represent standard deviation for 3 replicates (different capacitors/electrode pairs); error bars for the given value represent the tolerance provided by the manufacturer. In bright field images, the projected light patterns are red, the electrodes appear green, the space between them appears blue, and manipulations were in conc. PEGDA diluted 1:4 in DI water.

After clarifying the trap profile and the accuracy for the positioning of solder beads in the OET system, we explored the capacity for top-down assembly of solder beads to form conductive traces to bridge isolated electrodes, a common proof-of-concept used to evaluate electronic assembly/construction.[50-52] As described in the supplementary information file, an array of electrodes was formed on an OET bottom plate, each insulated from the a-Si:H layer below, and each pair separated by a gap (in space) of 100 μm (Figure S5). Figure 6(a) shows the goal – a line of solder beads connecting two formerly isolated electrodes. As illustrated in Movie S5 and Figure 6(b), it is straightforward to use OET to align the beads in what we call a "top down" mode, in which individual particles are picked and placed precisely, as needed. As illustrated in Figure 6(c)-(e), the pattern can be made permanent and conductive by photocuring, drying, and annealing, and finally, as shown in Figures 6(f) and 6(g), the resistances between the isolated metal contacts before and after assembling the solder beads (with annealing) were measured to be around 10^{13} Ω (noise floor) and 6.7 Ω, respectively. These results demonstrate the potential for using OET manipulation to assemble, interconnect, and create micro-electronics that are permanently assembled in a UV-cured polymer.

As a final step to build microcircuit, we explored the capacity of the technique to position and affix a thin-film microcapacitor to form a capacitive circuit. As shown in Figure 6(h), the unit tested here is 400 μm x 200 μm x 170 μm (l x w x h), and comprises a dielectric region in the center flanked by conductive terminals bearing solder on each side. As shown in Movie S6, clip 1, in initial tests with a simple, stationary rectangular light pattern, the capacitor was found to exhibit oscillatory behavior, repeatedly swinging from side-to-side. We hypothesize that this interesting behavior arises from the Janus-like nature of the partle, which likely experiences positive DEP on its conductive ends and negative DEP in the center. As shown in Move S6 clips 2-3 and Fig. 6 (i)-(j), stable control was achieved over the microcapacitor by projecting a custom "positive/negative cage" pattern into the chamber. To the best of our knowledge, this is the largest (0.0136 mm^3) and heaviest object (0.04 mg) that has been reported to be controllable by any optical micromanipulation technique previously. The maximum linear velocity and angular velocity of the microcapacitor when manipulated in this manner were found to scale with the applied bias voltage [Figure 6(k)], similar to the objects that experience only positive or negative DEP force.[34]As illustrated in Figure 6(l)-(o), the techniques described here can be used to position a microcapacitor such that it bridges isolated electrodes in a microelectronic circuit, and that this can be made permanent and functional by photocuring, drying and annealing. Finally, as shown in Figure 6(p), the capacitance of such structures were measured to be around 0.86 pF, close to the value given by the manufacturer (0.80 pF). As far as we are aware, this is the first report of the assembly of a microcapacitive circuit using optical micromanipulation techniques, which suggests utility for a wide range of applications in the future.

Conclusion

In this work, we demonstrated how OET can be used to assemble nano-/micro-materials to form tailored, artificial microstructures, which can then be immobilized/preserved in photocurable hydrogels via *in situ* photopolymerization. The system is easy-to-use with a user-friendly computer interface. We demonstrated that carbon/silver nanoparticles, graphene nanoplatelets and polystyrene micro-particles can be assembled to form TMPs in cured hydrogel structures, which can then be transferred to alternate substrates. In addition, the method was demonstrated to be useful for forming conductive structures to bridge isolated metal electrodes, and assembly of capacitive components. This work demonstrates great potential for using OET and *in situ* photopolymerisation for assembly and building microstructures and micro-electronics on demand.

Methods

Instrumentation and devices: The instrument used in this work is similar to one reported previously,[34] featuring a projector interfaced to an upright microscope (Leica DM 2000 with motorized stage Märzhäuser Scan Plus 100×100). In this work, the projector is a Polygon DMD Illuminator (Mightex Inc.) with two independently controlled LED light sources at 380 nm (UV) and 620 nm (red), respectively, with intensities and other parameters given in the supplementary information. The OET device used in this work comprised a 30 μL fluidic chamber sandwiched in between a top and a bottom plate using 150 μm thick double sided tape (3M 9965). Each plate was formed from a glass slide coated with 200-nm-thick ITO, with the bottom plate featuring an additional photoconductive layer of 1 μm thick a-Si:H, deposited by plasma enhanced chemical vapor deposition (PECVD)[28]. In some cases (e.g. Figure 6), metal electrodes were fabricated on top of the a-Si:H layer of the bottom plate (see Supporting Information and Figure S5 for fabrication details). OET devices were driven by applying a sine-wave bias between the top and bottom plates. For most experiments, the bias was 15 Vpp at 20 kHz; for those involving the manipulation of microcapacitors, the bias varied, but typically was 25 Vpp at 20 kHz.

Preparation of hydrogel solution for photopolymerization: A hydrogel pre-polymer solution was prepared by dissolving PEGDA (Sigma-Aldrich, 455008) and poly(ethylene glycol) (PEG, Sigma-Aldrich, 202398) into deionized (DI) water containing 0.05% (v/v) Tween 20 (Sigma-Aldrich, P2287). The composition was 30% (v/v) PEGDA, 40% (v/v) PEG, and 30% (v/v) DI water (with Tween 20). Finally, 0.5% (w/v) diphenyl(2,4,6-trimethylbenzoyl)-phosphine oxide (TPO, Sigma-Aldrich, 906808) was dissolved in the hydrogel solution, which functions as photoinitiator to trigger the UV-activatable crosslinking reaction. This mixture was known as the "concentrated PEGDA solution", which was diluted in different ratios in DI water containing 0.05% (v/v) Tween 20 for most applications. The conductivity and viscosity of a 1:4 dilution of concentrated PEGDA was measured to be 1.8×10^{-2} S/m and 7.6×10^{-3} Pa·s, respectively.

Measurement of curing time and curing percentage for solutions with different ratios of concentrated

PEGDA to DI water: In each experiment, a solid rectangular light pattern (900 μm by 550 μm) was projected into an OET device filled with a solution of PEGDA. The cured region could be identified manually by a change in contrast, and UV illumination was continuously applied for a duration of t_{ill} seconds, and turned off when the first of the following conditions were met: (1) the cured hydrogel structure completely covered the illuminated region, or (2) the cured region did not show an observable change or expansion for 90 s. The curing time for each condition was then recorded as t_{ill} for (1) and t_{ill} - 90 s for (2). After curing, the percentage of the cured area (compared to the area of the UV light pattern) was calculated using ToupView software (ToupTek Photonics). The curing time and curing percentage were measured five times per condition on five different devices. When following the conditions indicated above (which ensured that the chamber was not overexposed), the fluid in the remainder of the chamber was not affected, such that additional photopolymerized structures could be formed.

Preparation of samples for OET manipulation: Two kinds of polystyrene microspheres (with nominal average diameters provided by the supplier, Polysciences) were used in this work: 10 μm dia. plain microbeads (Polysciences, 17136), and 6 μm dia. red fluorescent microbeads (Polysciences, 19111), which were provided by the supplier as aqueous suspensions and then centrifuged and resuspended at 0.1 to 1×10^7 particles mL^{-1} in DI water containing 0.05% (v/v) Tween 20. Carbon nanoparticles (Sigma-Aldrich, 633100), silver nanoparticles (Sigma-Aldrich, 576832), graphene nanoplatelets (Sigma-Aldrich, 799084), and solder microbeads (15 to 25 μm spheres of $Sn_{96.5}Ag_3Cu_{0.5}$ from Industrie des Poudres Sphériques) were provided in powder form by the supplier. These materials were suspended (separately) at 0.1 to 1×10^6 particles mL^{-1} in DI water containing 0.05% (v/v) Tween 20. Prior to each experiment, the relevant suspension of nano-/micro-materials was sonicated using an ultrasonic probe (Sonics & Materials Inc., VCX 130) for five minutes, and then it was mixed at various ratios (most often 4:1) with concentrated PEGDA solution. Finally, in each microcapacitor experiment, 0.80 pF thin-film capacitors (C005YK0R8PBSTR, AVX Corporation) were suspended in in DI water containing 0.05% (v/v) Tween 20 diluted 4:1 with concentrated PEGDA).

Bottom-up TMP assembly, harvesting, and transfer: 30 μL of a homogenous suspension of particles in diluted PEGDA solution was loaded into the OET device. The desired red-light pattern was projected into the system until particle assembly was observed (typically within 60 s). The OET device was submerged vertically in a beaker in DI water solution for 2 minutes. The OET device was then removed and placed in an oven at 50 C^o for 3 minutes. After drying, the OET top plate was gently removed, leaving the cured hydrogel microstructure with the assembled TMP on the surface of the OET bottom plate. TMPs were then transferred to other destination substrates using the method reported previously.[29] Harvested, transferred TMPs were characterized by bright-field microscopy or scanning electron microscopy (see the Supporting Information for details for the latter). Some fluorescent TMPs were characterized by fluorescence microscopy.

Top-down particle manipulation experiments: For experiments with polystyrene microparticles or solder

microbeads, 20 μL of the solution without microparticles was pipetted into the chamber of the OET device, followed by another injection of 10 μL of the same solution with microparticles. This arrangement allows for a region of the chamber to be free of microparticles, providing space for manipulation. For polystyrene particles, a doughnut-shaped red-light pattern (with inner and outer diameter 100 μm and 160 μm, respectively) was used to select and isolate an individual particle as in Figure 2(a)-(b), The particle was moved by keeping the light pattern stationary while translating the motorized microscope stage (and OET device) at a known velocity. To measure maximum velocity, the translational velocity of the motorized stage was gradually increased until the DEP force exerted on the particle could no longer match the viscous drag force such that the particle escaped from the light pattern, as described previously[44]. The highest velocity that allowed successful bead transport was defined as its maximum moving velocity. For each condition evaluated, this property was measured for 5 movable particles on 5 different devices. In each such experiment, 20 particles (on a given device) were also tested for a “yes” or “no” measurement of 'movability' (at 1 μm/s). The percentage of movable particles was calculated from the 20 tests, which were repeated five times on five different devices. For solder microbeads, a red-light circular light pattern (with 30 μm diameter) was used to select and isolate an individual particle as in Figure 5(a)-(b). Each particle's radius was measured and was moved at a given translational velocity (by moving the stage, as above), recording the center-to-center distance *D* between the light pattern and the particle. *D* was measured for 10 particles per velocity and was used to estimate the DEP force experienced by the particle according to equation (1). Since the solder beads have a density of 8 g/cm^3, and the DEP force also pulls them to the bottom of the OET chamber, Faxen’s correction was applied to the estimate, as described previously for other materials.[45,46] To measure the positioning accuracy of solder beads, in each experiment, a bead was initially confined in a 30-μm-diameter circular (red-light) OET trap. The position of the bead center relative to the trap center (in X- and Y-dimensions) was estimated using the microscope’s image analyzing software (ToupView 3.7). The trap was then moved to a destination position (with the X- and Y- coordinates of the destination selected randomly to be between 30-500 μm away from the initial trap-center coordinates) at 15 μm/s, after which the position of the bead center relative to the trap center was estimated again. The differences between the initial and final relative positions were then reported as "post-translation offsets." This process was repeated for 18 different beads. Finally, for each experiment with microcapacitors, a 30 μL aliquot of a 1:4 dilution of concentrated PEGDA containing a single microcapacitor was loaded into a device. A red-light pattern dubbed the "positive/negative cage" comprising four solid bars (two thick 250 μm x 110 μm bars separated by 210 microns arranged perpendicularly to two thin 210 μm x 45 μm bars separated by 270 microns) was projected into the OET device. This pattern was translated (by moving the microscope stage) and rotated (by rotating the projected image) until the large bars covered the solder-coated edges of the capacitor, and the thin bars were just outside of the non-coated edges of the capacitor. Maximum linear velocity and angular velocity for microcapacitors were determined using methods described previously for other particles.[34]

Top-down assembly of microelectronic circuit components: Microelectronic circuits were formed by

loading either a suspension of solder beads or a single microcapacitor a 1:4 dilution of concentrated PEGDA into modified OET devices bearing isolated electrodes with 100 μm gap (fabricated as described in the supplementary information file and Figure S5). For solder beads, rectangular red-light patterns (30 μm by 20 μm, or 20 μm by 25 μm) were used to collect and position solder beads between a pair of electrodes, one-by-one, by manipulating the microscope stage relative to the projected pattern. As each solder bead was added to the structure, the light pattern used to position it was kept "on" and immobile, holding the structure in place while the next solder bead was collected. The structure was then cured as described above, and the device was submerged vertically in a beaker in DI water solution for 2 minutes and then dried in an oven (50^{o}C for 3 minutes). Finally, the solder was annealed on a hotplate at 220^{o}C for 2 minutes. The current-voltage (I-V) characteristics of pairs of electrodes in devices before and after forming solder-bead electrical traces were determined using a semiconductor device analyzer/probe station (Keithley 4200 SCS). For microcapacitor manipulation, the positive/negative cage pattern was projected into the device, and a combination of translation and rotation steps (described above) was used to position the capacitor such that it bridged a pair of isolated electrodes. The circuit was then cured, dried and annealed as described above for the solder beads. The capacitance of pairs of electrodes on three different devices bridged by three different capacitors was measured using a capacitance meter (Model 3000, GLK Instruments).

Supporting Information

Descriptions and figures illustrating the computer/projector interface used to generate light patterns, additional examples of assembled/cured TMPs, SEM images of nano-/micro- materials used to assemble TMPs, the 3D simulation model, the fabrication process-flow for forming metal contacts, as well as descriptions of supplementary movies are provided in the Supporting Information file.

Acknowledgements

This research was supported by the Natural Sciences and Engineering Research Council of Canada (Grant Nos. RGPIN 2019-04867, CREATE 482073-16, ALLRP 548593-19, and RTI-2019-00300), as well as the National Natural Science Foundation of China (Grant Nos. 11774437, 61975243) and Local Innovative and Research Teams Project of Guangdong Pearl River Talents Program (Grant No. 2017BT01X121). The authors acknowledge the support from the Centre for Nanostructure Imaging at the Department of Chemistry, University of Toronto for assistance in collecting SEM images, and the Centre for Research and Applications in Fluidic Technologies (CRAFT) for assistance in device fabrication, and CMC Microsystems for providing COMSOL license. The authors also acknowledge the support of Nancy Khuu (Department of Chemistry, University of Toronto) and Dr. Alexander Baker (Donnelly Centre for Cellular and Biomolecular Research, University of Toronto) for assistance with rheology measurements. S. Zhang acknowledges the RBC Post-Doctoral Fellowship program. A.R.W. acknowledges the Canada Research Chair (CRC) program.

Author contributions

S. Z. and W. L. conceived the idea and carried out the OET experiments. S.Z and M. E. built the experimental setup. W. L. and J. P. prepared and optimized the sol-form PEGDA solution. Y. C. and Y. Z. deposited the a-Si:H materials. S. Z., M. E. and M. S. fabricated the OET devices. Y. Z., W. D., and T. W. performed the IV measurement. S. Z. and A. R. W. wrote the manuscript. All authors discussed the results and commented on the manuscript. Y. S., N.P.K., S. L. N. and A. R. W. coordinated and supervised the project.

Conflict of Interest

The authors declare no conflict of interest.

References

1. A. Carlson, A. M. Bowen, Y. Huang, R. G. Nuzzo, J. A. Rogers, "Transfer printing techniques for materials assembly and micro/nanodevice fabrication", *Adv. Mater.* 24(39), 5284-5318 (2012).
2. M. A. Meitl, Z. T. Zhu, V. Kumar, K. J. Lee, X. Feng, Y. Y. Huang, I. Adesida, R. G. Nuzzo, J. A. Rogers, "Transfer printing by kinetic control of adhesion to an elastomeric stamp", *Nat. Mater.* 5(1), 33-38 (2006).
3. T. H. Kim, K. S. Cho, E. K. Lee, S. J. Lee, J. Chae, J. W. Kim, D. H. Kim, J. Y. Kwon, G. Amaratunga, S. Y. Lee, B. L. Choi, "Full-colour quantum dot displays fabricated by transfer printing", *Nat. Photon.* 5(3), 176-182 (2011).
4. Y. Zhang, B. K. Chen, X. Y. Liu, Y. Sun, "Autonomous robotic pick-and-place of micro objects," *IEEE. Trans. Robot.* 26(1), 200-207 (2010).
5. B. K. Chen, Y. Zhang, Y. Sun, "Active release of microobjects using a MEMS microgripper to overcome adhesion forces," *J. Microelectromech. Syst.* 18(3), 652-659 (2009).
6. D. Jevtics, A. Hurtado, B. Guilhabert, J. McPhillimy, G. Cantarella, Q. Gao, H. H. Tan, C. Jagadish, M. J. Strain, M. D. Dawson, "Integration of semiconductor nanowire lasers with polymeric waveguide devices on a mechanically flexible substrate", *Nano Lett.* 17(10), 5990-5994 (2017).
7. B. Guilhabert, A. Hurtado, D. Jevtics, Q. Gao, H. H. Tan, C. Jagadish, M. D. Dawson, "Transfer printing of semiconductor nanowires with lasing emission for controllable nanophotonic device fabrication", *ACS Nano* 10(4), 3951-3958 (2016).
8. A. J. Trindade, B. Guilhabert, E. Y. Xie, R. Ferreira, J. J. McKendry, D. Zhu, N. Laurand, E. Gu, D. J. Wallis, I. M. Watson, C. J. Humphreys, "Heterogeneous integration of gallium nitride light-emitting diodes on diamond and silica by transfer printing", *Opt. Exp.* 23(7), 9329-9338 (2015).
9. J. E. Melzer, E. McLeod, "3D Nanophotonic device fabrication using discrete components", *Nanophotonics* 9(6), 1373–1390 (2020).
10. A. Ashkin, J. M. Dziedzic, T. Yamane, "Optical trapping and manipulation of single cells using infrared laser beams", *Nature* 330(6150), 769-771 (1987).
11. D. G. Grier, "A revolution in optical manipulation", *Nature* 424(6950), 810-816 (2003).
12. K. Dholakia, T. Čižmár, "Shaping the future of manipulation", *Nat. Photon.* 5(6), 335-342 (2011).
13. M. Daly, M. Sergides, S. N. Chormaic, "Optical trapping and manipulation of micrometer and submicrometer particles", *Laser. & Photon. Rev.* 9(3), 309-329 (2015).
14. L. Lin, X. Peng, X. Wei, Z. Mao, C. Xie, Y. Zheng, "Thermophoretic Tweezers for Low-Power and Versatile Manipulation of Biological Cells", *ACS Nano* 11(3), 3147−3154(2017).
15. L. Lin, J. Zhang, X. Peng, Z. Wu, A. C. H. Coughlan, Z. Mao, M. A. Bevan, Y. Zheng, "Opto-

Thermophoretic Assembly of Colloidal Matter", *Sci. Adv.* 3(9), e1700458 (2017).
16. L. Lin, M. Wang, X. Peng, E. N. Lissek, Z. Mao, L. Scarabelli, E. Adkins, S. Coskun, U. Sahin, H. E. Unalan, B. A. Korgel, L. M. Liz-Marzán, E. L. Florin, Y. Zheng, "Opto-thermoelectric nanotweezers", *Nat. Photon.* 12(4), 195-201 (2018).
17. M. Jubera, I. Elvira, A. García-Cabañes, J. L. Bella, M. Carrascosa, "Trapping and patterning of biological objects using photovoltaic tweezers", *Appl. Phys. Lett.* 108(2), 023703 (2016).
18. M. Carrascosa, A. García-Cabañes, M. Jubera, J. B. Ramiro, F. Agulló-López, "LiNbO3: A photovoltaic substrate for massive parallel manipulation and patterning of nano-objects", *Appl. Phys. Rev.* 2(4), 040605 (2015).
19. I. Elvira, J. F. Muñoz-Martínez, Á. Barroso, C. Denz, J. B. Ramiro, A. García-Cabañes, F. Agulló-López, M. Carrascosa, "Massive ordering and alignment of cylindrical micro-objects by photovoltaic optoelectronic tweezers", *Opt. Lett.* 43(1), 30-33 (2018).
20. A. Puerto, A. Méndez, L. Arizmendi, A. García-Cabañes, M. Carrascosa, "Optoelectronic Manipulation, Trapping, Splitting, and Merging of Water Droplets and Aqueous Biodroplets Based on the Bulk Photovoltaic Effect", *Phys. Rev. Appl.* 14(2), 024046 (2020).
21. M. C. Wu, "Optoelectronic tweezers", *Nat. Photon.* 5(6), 322-324 (2011).
22. P. Y. Chiou, A. T. Ohta, M. C. Wu, "Massively parallel manipulation of single cells and microparticles using optical images", *Nature* 436(7049), 370-372 (2005).
23. H. Hwang, J. K. Park, "Optoelectrofluidic platforms for chemistry and biology", *Lab Chip* 11(1), 33-47 (2011).
24. W. Liang, L. Liu, J. Wang, X. Yang, Y. Wang, W. J. Li, W. Yang, "A Review on Optoelectrokinetics-Based Manipulation and Fabrication of Micro/Nanomaterials", *Micromachines* 11(1),78 (2020).
25. Y. Huang, Z. Liang, M. Alsoraya, J. Guo, D. E. Fan, "Light Gated Manipulation of Micro/Nanoparticles in Electric Fields", *Adv. Intell. Syst.* 2, 1900127 (2020).
26. M. B. Lim, R. G. Felsted, X. Zhou, B. E. Smith, P. J. Pauzauskie, "Patterning of graphene oxide with optoelectronic tweezers,"*Appl. Phys. Lett.* 113(3), 031106 (2018).
27. M. B. Lim, J. L. Hanson, L. Vandsburger, P. B. Roder, X. Zhou, B. E. Smith, F. S. Ohuchi, P. J. Pauzauskie, "Copper-and chloride-mediated synthesis and optoelectronic trapping of ultra-high aspect ratio palladium nanowires", *J. Mater. Chem. A.* 6(14), 5644-5651 (2018).
28. S. Zhang, N. Shakiba, Y. Chen, Y. Zhang, P. Tian, J. Singh, M. D. Chamberlain, M. Satkauskas, A. G. Flood, N. P. Kherani, S. Yu, P. W. Zandstra, A. R. Wheeler, "Patterned Optoelectronic Tweezers: A New Scheme for Selecting, Moving, and Storing Dielectric Particles and Cells", *Small* 14(45), 1803342 (2018).
29. S. Zhang, Y. Zhai, R. Peng, M. Shayegannia, A. G. Flood, J. Qu, X. Liu, N. P. Kherani, A. R. Wheeler, "Assembly of Topographical Micropatterns with Optoelectronic Tweezers", *Adv. Opt. Mater.* 7(20), 1900669 (2019).
30. W. Liang, L. Liu, S. H. Lai, Y. Wang, G. B. Lee, W. J. Li, "Rapid assembly of gold nanoparticle-based microstructures using optically-induced electrokinetics", *Opt. Mater. Express* 4(11), 2368-2380 (2014).
31. S. Liang, Y. Cao, Y. Dai, F. Wang, X. Bai, B. Song, C. Zhang, C. Gan, F. Arai, L. Feng, "A Versatile Optoelectronic Tweezer System for Micro-Objects Manipulation: Transportation, Patterning, Sorting, Rotating and Storage", *Micromachines* 12(3), 271 (2021).
32. J. Juvert, S. Zhang, I. Eddie, C. J. Mitchell, G. T. Reed, J. S. Wilkinson, A. Kelly, S. L. Neale,

"Micromanipulation of InP lasers with optoelectronic tweezers for integration on a photonic platform", *Opt. Exp.* 24(16), 18163-18175 (2016).

33. S. Zhang, J. Juvert, J. M. Cooper, S. L. Neale, "Manipulating and assembling metallic beads with Optoelectronic Tweezers", *Sci. Rep.* 6, 32840 (2016).
34. S. Zhang, E. Y. Scott, J. Singh, Y. Chen, Y. Zhang, M. Elsayed, M. D. Chamberlain, N. Shakiba, K. Adams, S. Yu, C. M. Morshead, P. W. Zandstra, A. R. Wheeler, "The optoelectronic microrobot: A versatile toolbox for micromanipulation", *PNAS* 116(30), 14823-14828 (2019).
35. S. Zhang, Y. Liu, Y. Qian, W. Li, J. Juvert, P. Tian, J. C. Navarro, A. W. Clark, E. Gu, M. D. Dawson, J. M. Cooper, S. L. Neale, "Manufacturing with light - micro-assembly of opto-electronic microstructures", *Opt. Exp.* 25(23), 28838-28850 (2017).
36. R. Pethig, "Review Article - Dielectrophoresis: Status of the theory, technology, and applications", *Biomicrofluidics* 4(2), 022811(2010).
37. S. Zhang, W. Li, M. Elsayed, P. Tian, A. W. Clark, A. R. Wheeler, S. L. Neale, "Size-scaling effects for microparticles and cells manipulated by optoelectronic tweezers", *Opt. Lett.* 44(17), 4171-4174 (2019).
38. A. Jamshidi, P. J. Pauzauskie, P. J. Schuck, A. T. Ohta, P. Y. Chiou, J. Chou, P. Yang, M. C. Wu, "Dynamic manipulation and separation of individual semiconducting and metallic nanowires", *Nat. Photon.* 2(2), 86-89 (2008).
39. Z. Chen, F. Nan, Z. Yan, "Making permanent optical matter of plasmonic nanoparticles by in situ photopolymerization," *J. Phys. Chem. C* 124(7), 4215-4220 (2020).
40. X. Peng, J. Li, L. Lin, Y. Liu, Y. Zheng, "Opto-thermophoretic manipulation and construction of colloidal superstructures in photocurable hydrogels," *ACS Appl. Nano Mater.* 1(8), 3998-4004 (2018).
41. X. Zhou, Y. Hou, J. Lin, "A review on the processing accuracy of two-photon polymerization," *AIP Adv.* 5(3), 030701 (2015).
42. K. Salaita, S. W. Lee, X. Wang, L. Huang, T. M. Dellinger, C. Liu, C. A. Mirkin, "Sub-100 nm, centimeter-scale, parallel dip-pen nanolithography," *Small* 1(10), 940-945 (2005).
43. P. Y. Chiou, Interactive microparticle manipulation using OET [Video file], https://www.youtube.com/watch?v=_FkROvhVzCo&list=UUX6e2chk7w6xSDQLcdG1UKQ&index=19 (accessed: September 2019).
44. S. Zhang, A. Nikitina, Y. Chen, Y. Zhang, L. Liu, A. G. Flood, J. Juvert, M. D. Chamberlain, N. P. Kherani, S. L. Neale, A. R. Wheeler, "Escape from an optoelectronic tweezer trap: Experimental results and simulations", *Opt. Express* 26(5), 5300-5309 (2018).
45. S. L. Neale, M. Mazilu, J. I. Wilson, K. Dholakia, T. F. Krauss, "The resolution of optical traps created by light induced dielectrophoresis (LIDEP)", *Opt. Express* 15(20), 12619-12626 (2007).
46. S. B. Huang, M. H. Wu, Y. H. Lin, C. H. Hsieh, C. L. Yang, H. C. Lin, C. P. Tseng, G. B. Lee, "High-purity and label-free isolation of circulating tumor cells (CTCs) in a microfluidic platform by using optically-induced-dielectrophoretic (ODEP) force", *Lab Chip* 13(7), 1371-1383 (2013).
47. S. Zhang, Y. Liu, J. Juvert, P. Tian, J. C. Navarro, J. M. Cooper, S.L. Neale, "Use of optoelectronic tweezers in manufacturing—accurate solder bead positioning", *Appl. Phys. Lett.* 109(22), 221110 (2016).
48. X. Wang, X. B. Wang, P. R. C. Gascoyne, "General expressions for dielectrophoretic force and electrorotational torque derived using the Maxwell stress tensor method," *J. Electrostat.* 39(4), 277–295 (1997).

49. S. Kumar, P. J. Hesketh, “Interpretation of ac dielectrophoretic behavior of tin oxide nanobelts using Maxwell stress tensor approach modeling,” *Sensor Actuat. B Chem.* 161(1), 1198–1208 (2012).
50. R. J. Barsotti, M. D. Vahey, R.Wartena, Y. M. Chiang, J. Voldman, F. Stellacci, “Assembly of metal nanoparticles into nanogaps,” *Small* 3(3), 488–499 (2007).
51. N. Liu, W. Liang, J. D. Mai, L. Liu, G. B. Lee, W. J. Li, “Rapid fabrication of nanomaterial electrodes using digitally controlled electrokinetics”, *IEEE Trans. Nanotechnol.* 13(2), 245-253 (2014).
52. Y. H. Lin, K. S. Ho, C. T. Yang, J. H. Wang, C. S. Lai, “A highly flexible platform for nanowire sensor assembly using a combination of optically induced and conventional dielectrophoresis”, *Opt. Express* 22(11), 13811-13824 (2014).